Parallel transmit coil dimensions affect SAR sensitivity to motion at 7T.

Alix Plumley[1], Philip Schmid[1], Emre Kopanoglu[1]

1. Cardiff University Brain Research Imaging Centre (CUBRIC), School of Psychology, Cardiff University, Cardiff, UK

Synopsis: Subject motion in parallel-transmit (pTx) causes channels' electric field interference patterns to change, influencing SAR distributions. This can cause safety limits to be exceeded when SAR-constrained pulses are designed for one position, with reports of local-SAR more than tripling due to motion in the literature. Here, we investigate the effect of pTx coil geometry by simulating 6 differently sized coil models and testing SAR sensitivity at 19 displaced positions. While our results agree with those previously reported for the similar-sized coil, we generally observe lower SAR motion-sensitivity in larger coil models, and much higher sensitivity for the smallest coils.

Introduction:

Parallel transmission (pTx) can overcome B1+ inhomogeneity in 7T head imaging[1-3], however specific absorption rate (SAR) hotspots and associated tissue heating can exceed safety limits when head motion occurs due to constructive interference between channels[4-6]. Motion-induced increases in peak local-SAR of over 200% have been reported for multi-spoke pTx pulses, along with unpredictable changes in hotspot location[4].

Interference patterns depend on the coil as well as the load, therefore SAR depends on coil geometry[7-8]. Here, we investigate whether pTx coil element dimensions affect SAR motion-sensitivity. For this, we compare motion-induced SAR changes using simulations with 6 different coils.

Methods:

6 coil models (A: smallest, to F: largest) consisted of 8-channel loop arrays; the height, width (of loops), and radius (of array) of which varied ±25%, ±25%, and +25%, respectively, compared to the base model C (figure 1). For each coil model, 1 central, and 19 off-centre positions were simulated using the Ella model[9] in Sim4Life (ZMT, Zurich, Switzerland), totalling 120 datasets. SAR was reported as most sensitive to axial displacements[4], so we focus on these. Simulation parameters followed those in [4]. Positions were defined with respect to the array origin across coil models.

Pulses were designed to uniformly excite an axial slice in quadrature and pTx (1/2/3/5-spokes) modes (1-spoke is RF-shimming). Pulses were designed with an adaptation of [10-12] using B1-distributions at the central position for each coil. Pulses were not SAR-constrained, but RF power was penalized (along with magnitude excitation error) in the cost function (with Tikhonov regularization = 0.1). Separate pTx pulses were designed for 6 slices (figure 1), yielding 25 pulses per coil.

Motion-sensitivity was quantified as SAR at each off-centre position normalised by that at the corresponding central position (SAR_{centre}) for each coil respectively. Whole-head (gSAR) and peak 10-gram averaged local-SAR (psSAR) were evaluated at all positions using voxelwise and 10-g average Q-

(i)

(ii)

(iii)
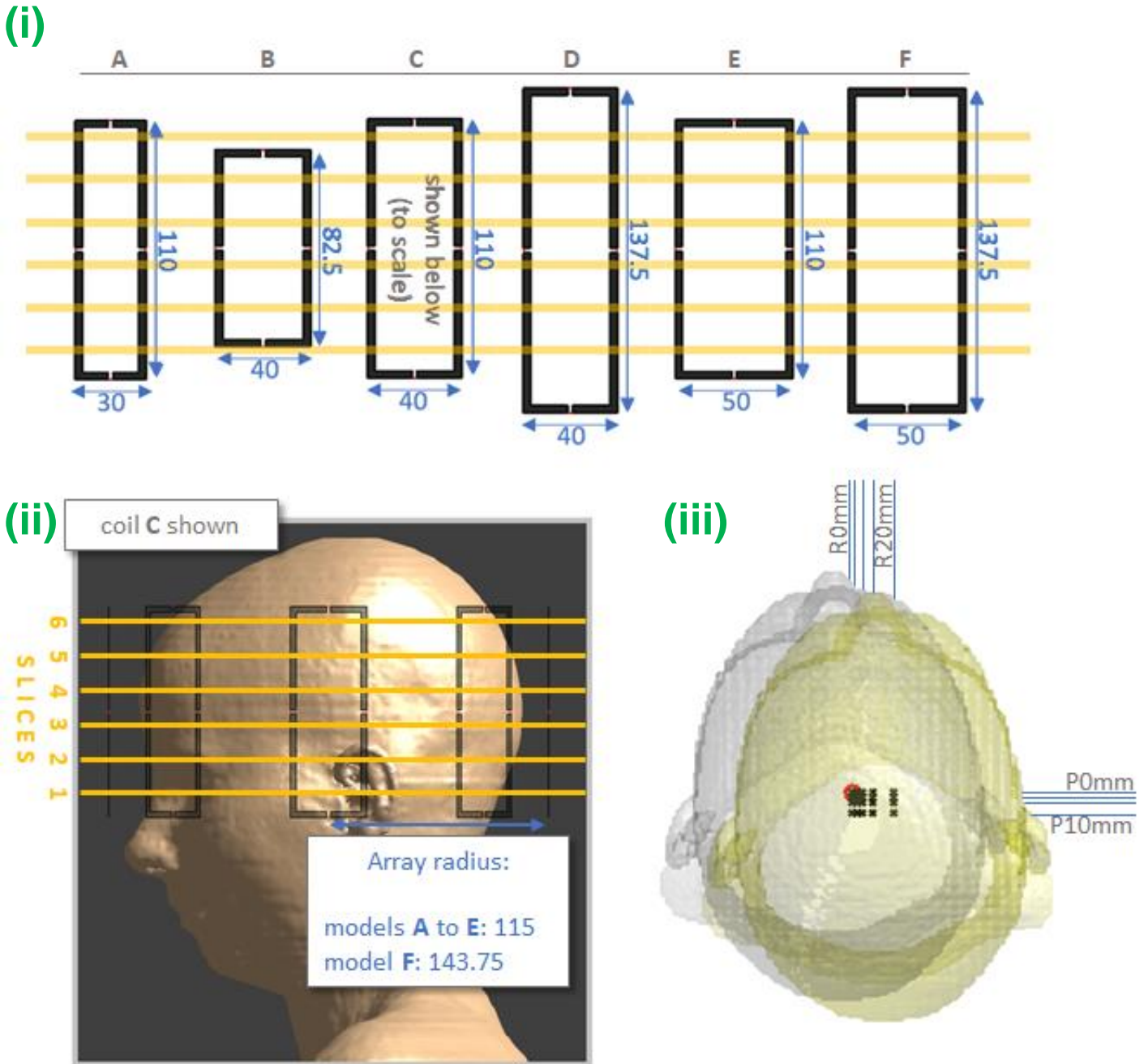
Figure 1. **(i)**: *Dimensions (in mm) of the 6 pTx coil models. A single loop (channel) is shown for each model.* **(ii)**: *Sagittal view of Sim4Life setup (coil model C shown). Slice positions -also shown in (i)- used for pulse design indicated in yellow. Slices remained constant in scanner coordinates across coil models.* **(iii)**: *Axial view of simulated positions. The 20 positions were combinations of: rightward: 0,2,5,10,20mm and posterior: 0,2,5, and 10mm. The two extremes (0,0 – grey) and (20,10 – yellow) are shown. The origins of all positions are indicated with crosses (with the central position's origin circled in red).*

matrices[13] respectively. Tissue volumes exposed to higher SAR than psSAR$_{centre}$ are also investigated (named 'high-SAR tissue' here). To exclude pulse design effects, eigenvalue-based SAR (eigSAR; assumes worst-case channel interferences) was also calculated using the 10-g Q-matrices.

Results & Discussion:

RF-shimming, slice 2
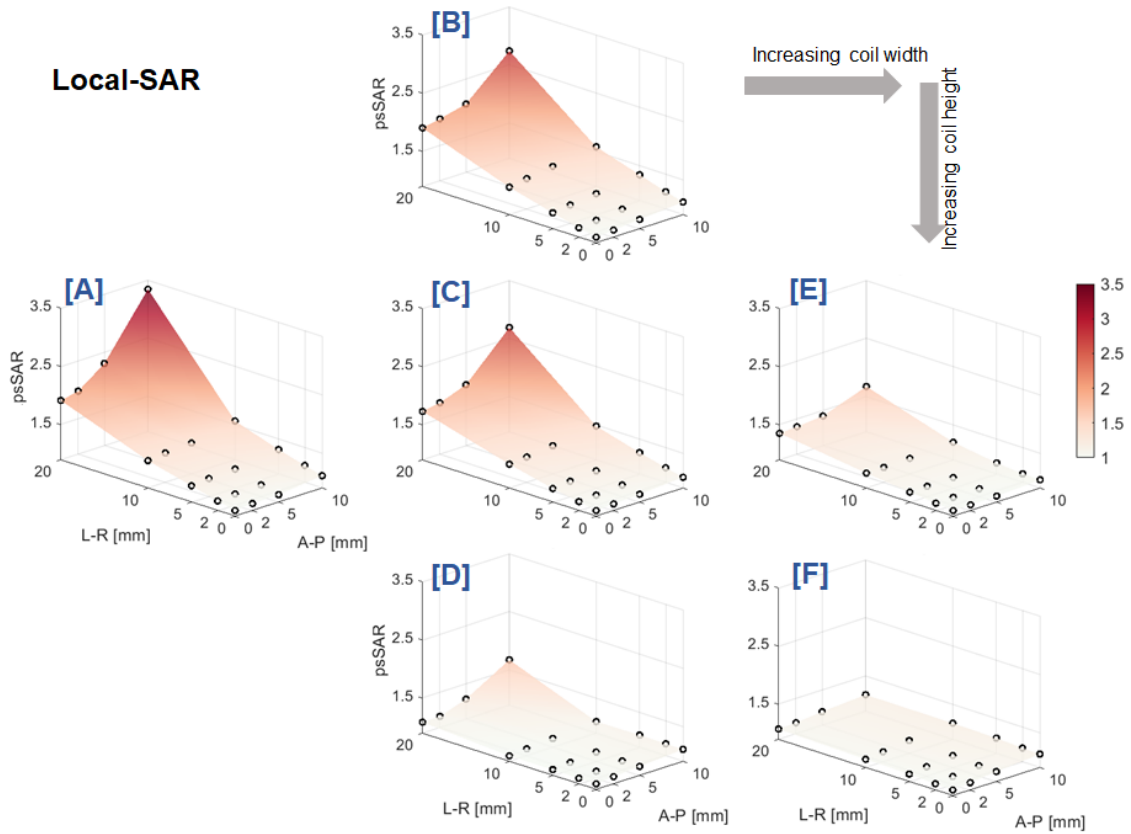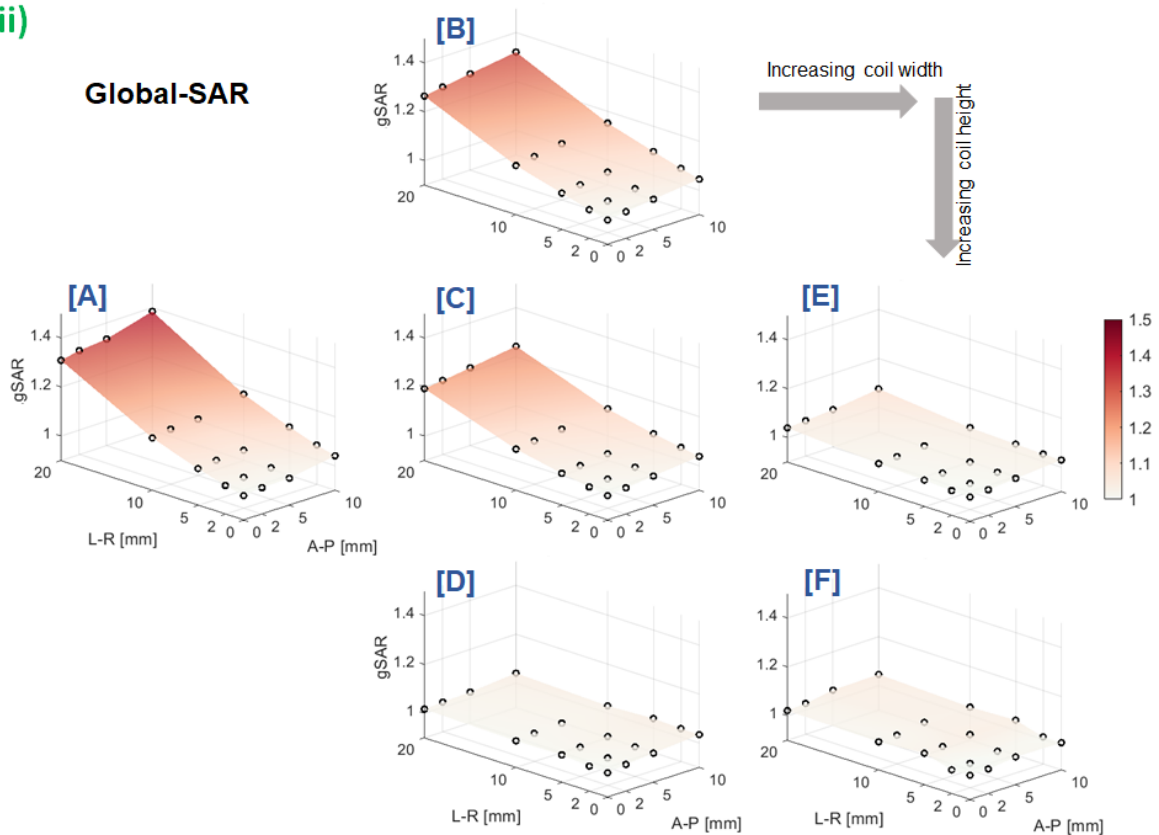
Figure 2. *Motion-sensitivity of peak local-SAR (**i**) and whole-head SAR (**ii**) for RF-shim pulses designed using slice 2 at the central position for each coil model A to F. Slices 2-5 showed similar trends. Y-axes refer to SAR at each evaluated position (left-right [L-R] and anterior-posterior [A-P] displacements), as a factor of SAR at the central position (i.e. without motion). SAR_centre was comparable across coil models (not shown).*

Coil C has similar dimensions to that in [4] and exhibited similar SAR-sensitivity to motion as expected F-shimming: 2.7 vs 2.4-fold psSAR increase). For the larger coils, psSAR sensitivity was lower, whereas for the smallest coil (A) we observed a much higher worst-case local-SAR increase of 3.8-fold. Similarly, coil C's eigSAR increased up to 43%, matching previous findings[4], however eigSAR was more motion-sensitive among smaller coil models (especially to posterior shifts) where it increased by 72%.

For pTx pulses, gSAR increased by up to 38% and 49% for RF-shim and multi-spoke pulses, respectively (both coil A). psSAR for RF-shimming was the most motion-sensitive metric, and was especially sensitive among smaller coils. psSAR increased by 3.8-fold, 2.7-fold, and 1.3-fold in the worst RF-shim case for coils A, C, and F, respectively. Figure 2 shows RF-shim SAR-sensitivity for a representative slice (slices 2-5 showed similar patterns, while 1 and 6 did not - discussed later). Figure 3 shows coils' worst cases across all pTx (including RF-shim) pulses. psSAR sensitivity and high-SAR tissue was lowest for the taller coil models, where psSAR increased by a maximum of 96% and 59% for coils D and F, respectively. As the number of spokes in pulses increases, SAR-sensitivity generally reduced and became more similar across coil models (figure 4.i), however the three largest coil models' worst-cases were multi-spoke pulses.

For quadrature pulses, gSAR was relatively stable, increasing by up to 5% (coil A). psSAR was most sensitive for coil C where it almost doubled, while psSAR for coils A and E increased by 18% and 5%, respectively (figure 5). Unlike pTx, in all quadrature worst-cases, the local-hotspot shifted from the front to back of the head. Even without motion, coil A experienced small, intense local-hotspots, meaning relative psSAR change was low when the hotspot shifted to a different location, but similar intensity. For large coils, fields were smoother throughout the head, leading to less intense hotspots even after motion. Coil C did not exhibit either behaviour, hence the largest relative increase.

For 14% of pulses, worst-case psSAR occurred at intermediate positions (ie. not the extremes). These pulses were for larger coils and/or slices 5 and 6, where psSAR sensitivity was lower. Coils D-F generally yielded less high-SAR tissue than smaller coils, with the biggest differences between coils seen for mid-axial slices (figure 4.ii).

SAR_{centre} (not shown) was higher when pulses were designed using slices 1 and 6. This is less concerning than motion-sensitivity of SAR, as SAR_{centre} can be constrained during pulse design. For coil B, these slices fell beyond the loops' vertical extent, and motion-sensitivity was notably lower than other slices (though $psSAR_{centre}$ was around threefold).

SAR for smaller pTx coils was generally more motion-sensitive than larger coils (wider or taller loops, and/or larger array radius). Maximum observed local-SAR increases due to motion were 3.8-fold and 1.6-fold for the smallest and largest coil models respectively. This is independent of pulse design, since eigenvalue-based SAR (which depends only on transmit *fields*) followed this pattern; however pTx pulses with small coils elicit the most concerning local-SAR increases.
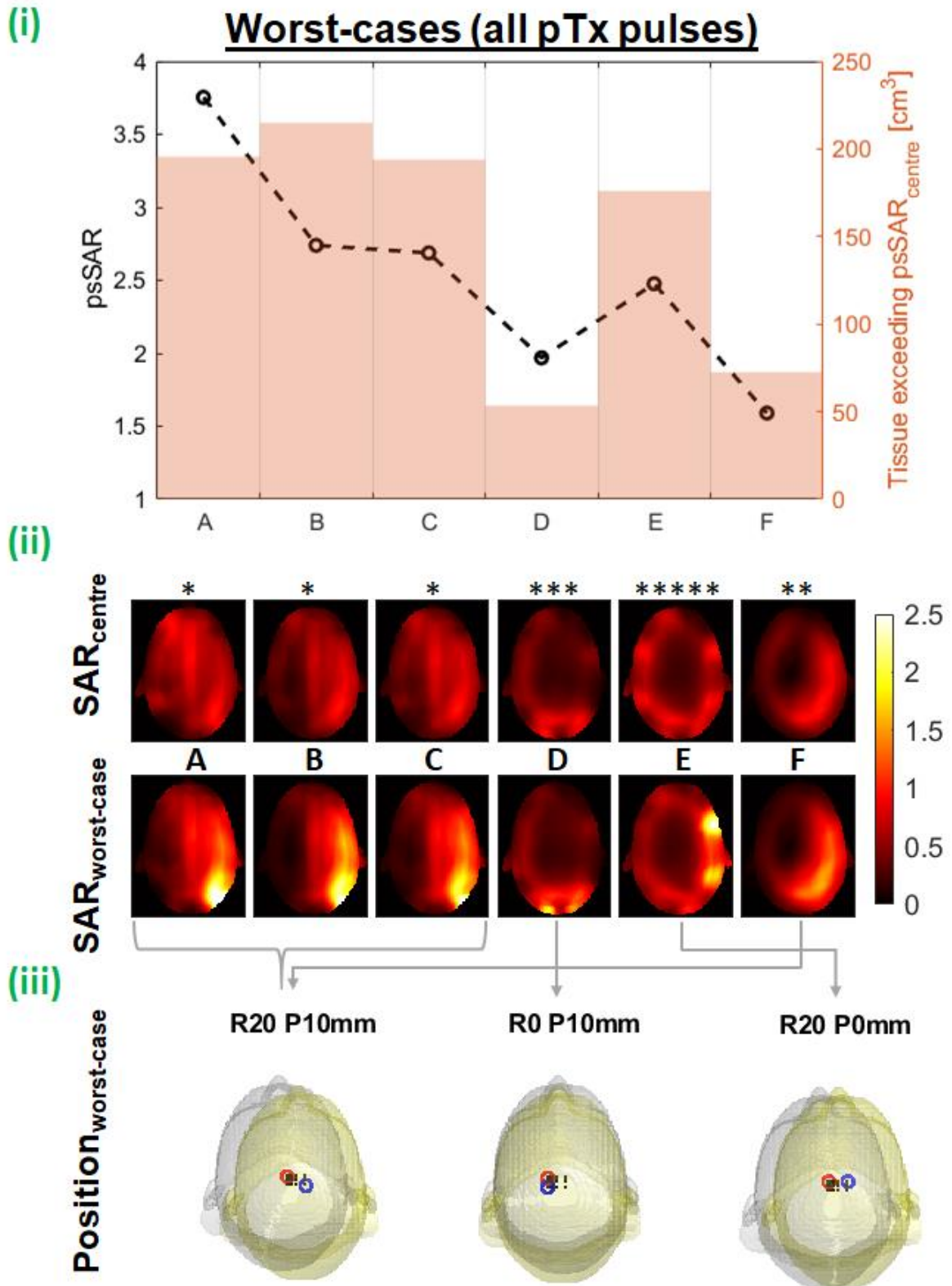
Figure 3. *Worst-case local-SAR following motion for pTx pulses.* **(i)**: *psSAR for worst-cases as a factor of psSAR$_{centre}$ (same pulse without motion). Tissue volume exposed to higher SAR than psSAR$_{centre}$ shown in orange.* **(ii)**: *SAR profiles for corresponding worst-cases (bottom row) compared to their SAR$_{centre}$ (top row). Colorbar shows psSAR as a factor of psSAR$_{centre}$ (normalised per coil). The number of spokes in each coil's worst-case pulse is indicated with asterisks.* **(iii)**: *The positions at which these worst-case psSAR were observed. All worst-cases were observed at slice 1 or 2.*
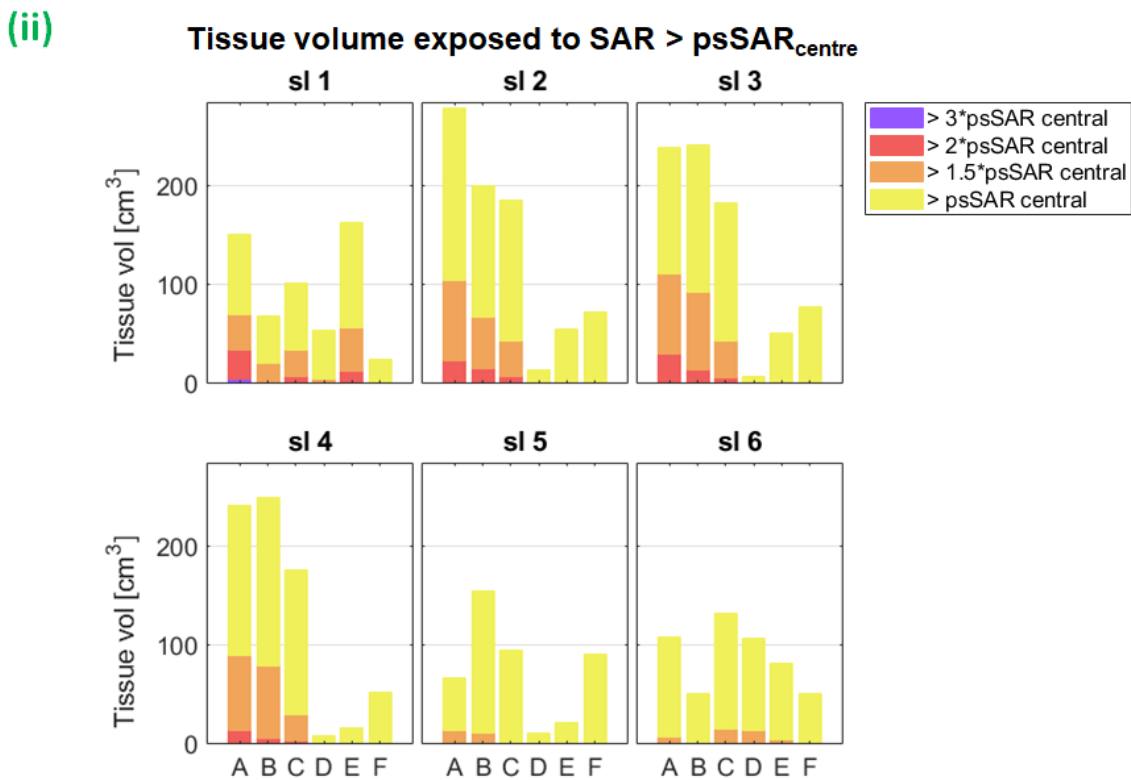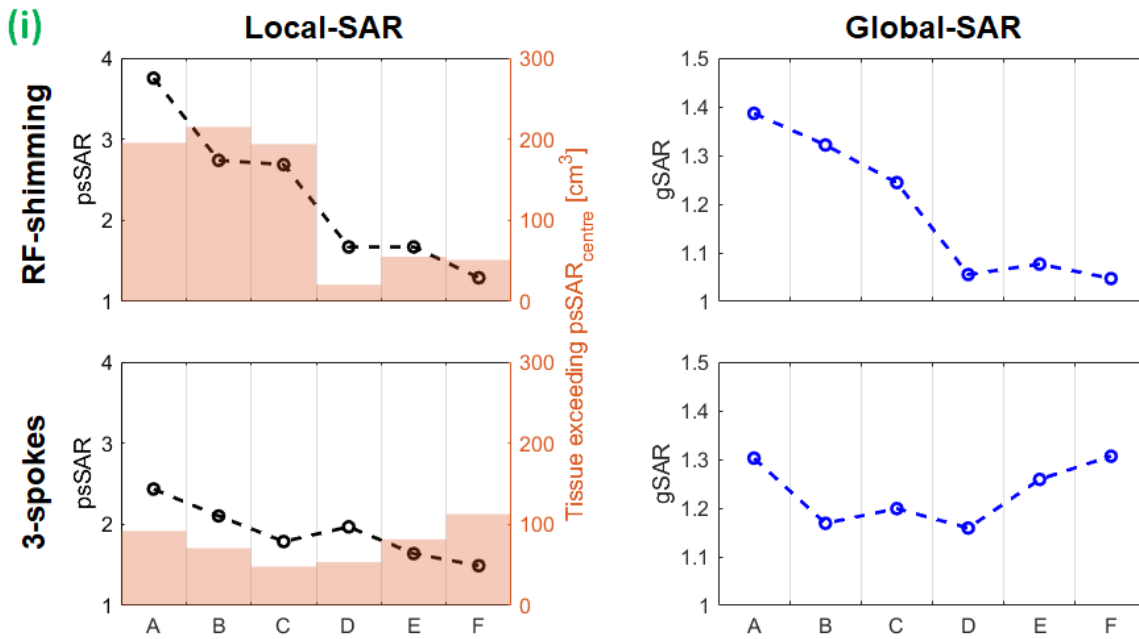
Figure 4. (i): *Local (psSAR; left) and global (gSAR; right) SAR for 1-spoke (top) and 3-spoke (bottom) pTx pulses for coil models A to F. Tissue volume exposed to >psSAR$_{centre}$ also shown. Worst-cases are defined by the largest increase in psSAR or gSAR for left and right figures respectively (i.e. the worst-case psSAR pulse was not necessarily the worst-case gSAR pulse).* **(ii):** *Tissue volumes exposed to higher SAR than psSAR$_{centre}$ by >100% (all colours), >150% (orange), >200% (red) and >300% (purple) for worst-case psSAR pTx pulses separated by slice (slices 1 to 6 shown in separate subplots).*
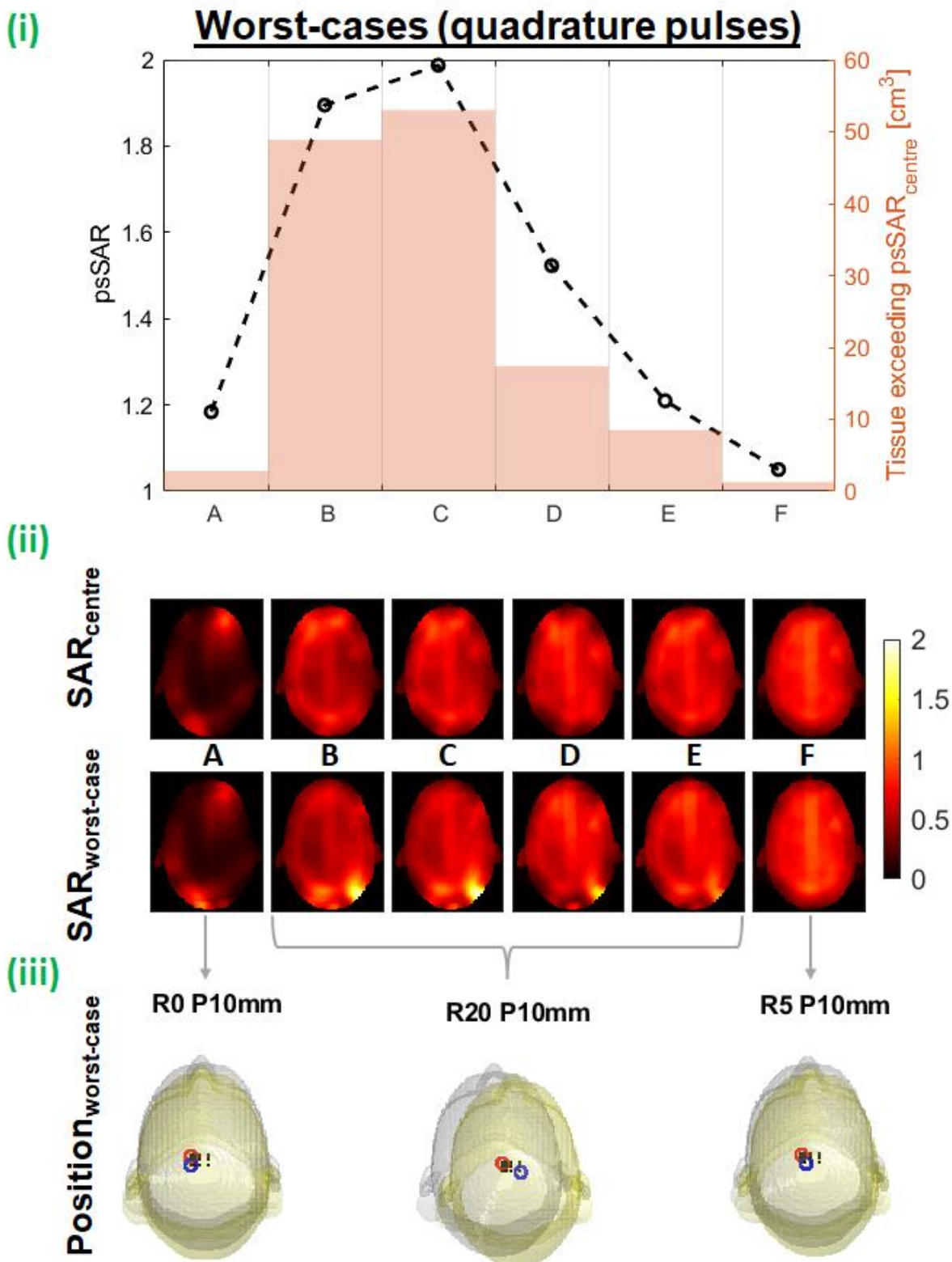
Figure 5. *Worst-case local-SAR following motion for quadrature pulses.* **(i)**: *psSAR for worst-cases as a factor of psSAR$_{centre}$ (same pulse without motion). Tissue volume exposed to higher SAR than psSAR$_{centre}$ shown in orange.* **(ii)**: *SAR profiles for corresponding worst-cases (bottom row) compared to their SAR$_{centre}$ (top row). Colorbar shows psSAR as a factor of psSAR$_{centre}$ (normalised per coil).* **(iii)**: *The positions at which these worst-case psSAR were observed. Relative psSAR across quadrature evaluations is independent of slice location.*

References

[1] J. Vaughan, et al., 7T vs. 4T: RF power, homogeneity, and signal-to-noise comparison in head images. *Mag Res Med,64 (1)*, pp. 24–30, 2001.

[2] U. Katscher and P. Bornert, Parallel RF transmission in MRI. *NMR Biomed,19 (3)*, pp. 393–400, 2006.

[3] C. M. Deniz, Parallel transmission for ultrahigh field MRI. *Topics in Mag Res Imag,28 (3),* pp. 159–171, 2019.

[4] E. Kopanoglu, et al., Specific absorption rate implications of within-scan patient head motion for ultra-high field MRI. Mag Res Med, 2020.

[5] S. Wolf, et al., SAR simulations for high-field MRI: How much detail, effort, and accuracy is needed? *Mag Res Med, 69 (4)*, pp. 1157–1168, 2013.

[6] N. Schon, et al., Impact of respiration on B1+ field and SAR distribution at 7T using a novel EM simulation setup. *Proc. Intl. Soc. Mag. Reson. Med., 28*, 2020.

[7] U. Katscher, et al., Basic considerations on the impact of the coil array on the performance of transmit sense. *Mag Res Mat Phys Biol Med, 18 (2)*, pp. 81–88, 2005.

[8] C. M. Deniz, et al., Radiofrequency energy deposition and radiofrequency power requirements in parallel transmission with increasing distance from the coil to the sample. *Mag Res Med, 75 (1)*, pp. 423–432, 2016.

[9] M-C. Gosselin, et al., Development of a new generation of high-resolution anatomical models for medical device evaluation: The virtual population 3.0. Phys Med Bio, *59 (18),* pp. 5287–5303, 2014.

[10] W. A. Grissom, et al, Advancing RF pulse design using an open-competition format: Report from the 2015 ISMRM challenge. *Mag Res Med*, 2016.

[11] ISMRM RF Pulse-design Challenge. http://challenge.ismrm.org/. 2016.

[12] W.A. Grissom, et al. Spatial domain method for the design of RF pulses in multicoil parallel excitation. *Mag Res Med, 56*(3), 620-629.

[13] I. Graesslin, et al., A specific absorption rate prediction concept for parallel transmission MR. *Mag Res Med, 68 (5),* pp. 1664–1674, 2012.